Chemical Engineering Science 126 (2015) 150–159

Contents lists available at ScienceDirect

Chemical Engineering Science

journal homepage: www.elsevier.com/locate/ces

Effects of dispersed phase viscosity on drop deformation and breakup in inertial shear flow

A.E. Komrakova [a,*], Orest Shardt [a], D. Eskin [b], J.J. Derksen [a,c]

[a] Chemical and Materials Engineering, University of Alberta, 7th Floor, ECERF, 9107 116 St., Edmonton, Alberta, Canada T6G 2V4
[b] Schlumberger DBR Technology Center, 9450 17 Ave. NW, Edmonton, Alberta, Canada T6N 1M9
[c] School of Engineering, University of Aberdeen, Aberdeen AB24 3UE, Scotland, UK

HIGHLIGHTS

- Behavior of a single liquid drop in simple shear flow at Re = 10 is studied.
- Numerical simulations are performed using a free energy lattice Boltzmann method.
- New results for drops that are less viscous than surrounding liquid.
- For each viscosity ratio the critical capillary number Ca_c is determined.
- Drop breakup processes are examined at $Ca \sim Ca_c$, $1.2Ca_c$, $1.5Ca_c$ and $2Ca_c$.

GRAPHICAL ABSTRACT

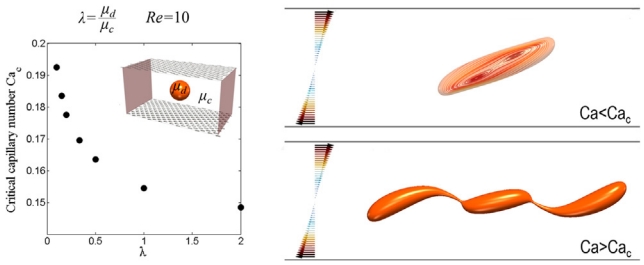

ARTICLE INFO

Article history:
Received 4 August 2014
Received in revised form
31 October 2014
Accepted 2 December 2014
Available online 16 December 2014

Keywords:
Drop deformation and breakup
Low viscosity dispersed phase
Lattice Boltzmann method
Binary liquid model

ABSTRACT

The deformation and breakup of a single liquid drop subjected to simple shear flow is studied numerically using a diffuse interface free energy lattice Boltzmann method. The effect of dispersed phase viscosity on the behavior of the drop at a drop Reynolds number Re = 10 is investigated over the range of viscosity ratios $\lambda = 0.1-2$ (dispersed phase viscosity over continuous phase viscosity) with a focus on $\lambda < 1$. For every λ the critical capillary number Ca_c for breakup is determined. For the range of λ considered, Ca_c decreases as λ increases. Both the extent of deformation and the breakup mechanism depend on the viscosity ratio and the capillary number. At the highest subcritical capillary number, the drop becomes less elongated and more inclined towards the vertical axis as the viscosity ratio increases. The changes in the drop breakup process are examined as the capillary number increases from the lowest supercritical $Ca \sim Ca_c$, to 1.2, 1.5 and $2Ca_c$. Drops break by the end-pinching mechanism, except for $\lambda = 2$ at $Ca = 2Ca_c$ where the drop undergoes capillary wave breakup.

1. Introduction

Studies of drop behavior in simple flow geometries have been used to interpret data on dispersion and emulsion formation due to more complex flow structures as they occur in process equipment (Rueger and Calabrese, 2013). While most experimental and simulation research has considered creeping flow (Grace, 1982; Rumscheidt and Mason, 1961; Stone, 1994; Rallison, 1984; Zhao, 2007; Marks, 1998), drops in complex flows, such as turbulence, can experience drop Reynolds numbers anywhere in the range 0.01–100 (Komrakova et al., 2014). To predict whether drops will break in turbulent flow, it is therefore necessary to understand how the conditions for breakup at moderate Reynolds numbers differ from those in creeping flow. While studies have considered the conditions for breakup in simple shear flow at Reynolds numbers up to 100 in systems with droplets that are as viscous

* Corresponding author.
E-mail address: komrakov@ualberta.ca (A.E. Komrakova).

http://dx.doi.org/10.1016/j.ces.2014.12.012
0009-2509/

or more viscous than the continuous phase (Renardy and Cristini, 2001a; Khismatullin et al., 2003), neither experiments nor simulations have been reported for the case of drops that are less viscous than their surroundings. This case is not unusual: for example, water droplets may be dispersed in a much more viscous oil (Rueger and Calabrese, 2013; Boxall et al., 2011). In the oil recovery industry, well productivity can be reduced by formation damages caused by oil-based emulsions that contain brine droplets (Fjelde, 2007). If a monodisperse emulsion is formed, then damage might occur even at low dispersed phase volume fractions. An understanding of deformation and breakup behavior of low-viscosity drops in a more viscous fluid will therefore fill an important gap in current knowledge with impact on industrial applications.

In the present work, the deformation and breakup of a single drop suspended in another liquid under simple shear flow is studied with numerical simulations using a free energy lattice Boltzmann method (Swift et al., 1996). The details of the method, its verification and validation can be found in Komrakova et al. (2014). Both liquids are Newtonian and of the same density. There are no surfactants or impurities in the system. The physical problem is determined by three dimensionless numbers: the drop Reynolds number $\mathrm{Re}=\dot{\gamma}a^2/\nu_c$, the capillary number $\mathrm{Ca}=a\dot{\gamma}\mu_c/\sigma$, and the viscosity ratio $\lambda=\mu_d/\mu_c$. Here, a is the undeformed drop radius; $\dot{\gamma}$ is the shear rate; ν_c is the kinematic viscosity of the continuous phase; μ_c, μ_d are the dynamic viscosities of the continuous and dispersed phases, respectively; and σ is the interfacial tension between the liquids.

The goal of this study is to investigate the behavior of a drop at a fixed Reynolds number $\mathrm{Re}=10$ over a range of viscosity ratios $\lambda=0.1-2$, with a focus on $\lambda<1$. For each λ it is necessary to determine the critical capillary number Ca_c that must be exceeded to break a drop. At subcritical capillary numbers, the drop achieves a steady final shape. The internal circulation patterns and the deformation parameters (elongation and orientation angle; see definitions below) are used to characterize the steady shape. When a supercritical capillary number is simulated, the drop breaks, and the breakup mechanism depends on the values of Ca and λ. Changes in the drop breakup process are examined as the capillary number increases from 20% above critical, to 50 and 100%.

The distinct characteristic of numerical simulations is that the entire deformation and breakup processes can be visualized revealing peculiarities of the events. However, in order to study physical processes numerically, it is necessary to select numerical parameters that produce trustworthy physical results. It was shown by Komrakova et al. (2014) that in addition to the three physical dimensionless numbers mentioned above (the Reynolds number, the capillary number and the viscosity ratio), two numerical dimensionless numbers have to be specified. In the diffuse interface method, which is used in this work, the finite thickness of the interface between the two liquids and related free energy model parameters are involved. These numerical degrees of freedom are characterized by two dimensionless numbers (van der Sman and van der Graaf, 2008): the interface Peclet number Pe and the Cahn number Ch. The interface Peclet number $Pe=\dot{\gamma}a\xi/(MA)$ relates the convection time scale to the interface diffusion time scale. The Cahn number $Ch=\xi/a$ is the ratio of the interface thickness and drop radius. Here, ξ is the interface thickness, M is the mobility, and A is a free energy model parameter. In the present study, the guidelines as developed by Komrakova et al. (2014) have been applied to specify Pe and Ch.

The rest of the paper is organized as follows. In Section 2 a brief description of the numerical method and its implementation are presented. In Section 3 the ability of the method to compute flows over the required range of viscosity ratios is demonstrated. The results of drop deformation and breakup are presented in Section 4. Conclusions are drawn in Section 5.

2. Numerical method and its implementation

The behavior of a drop in shear flow is studied numerically with the diffuse interface free energy lattice Boltzmann method (LBM) developed by Swift et al. (1996). The details of diffuse interface (or phase field) methods can be found in Jacqmin (1999), Yue et al. (2004), and Ding et al. (2007); our implementation of the method is presented in Komrakova et al. (2014). In particular, the interface between the two components is represented by a thin transition region with a finite thickness in which the composition varies smoothly. The composition of the system is described by the order parameter ϕ which is the relative concentration of the two components (Cahn and Hilliard, 1958; Penrose and Fife, 1990; Badalassi et al., 2003). To simulate the fluid dynamics of the binary mixture, the continuity and momentum equations are solved in conjunction with the convection–diffusion equation for the order parameter proposed by Cahn and Hilliard (1958, 1959). Thus, the evolution of density, velocity and order parameter are governed by the continuity, momentum, and convection–diffusion equations (Swift et al., 1996):

$$\partial_t\rho+\partial_\alpha(\rho u_\alpha)=0 \tag{1a}$$

$$\partial_t(\rho u_\alpha)+\partial_\beta(\rho u_\alpha u_\beta)=-\partial_\beta P^{th}_{\alpha\beta}+\partial_\beta\nu\left(\rho\partial_\alpha u_\beta+\rho\partial_\beta u_\alpha\right) \tag{1b}$$

$$\partial_t\phi+\partial_\alpha(\phi u_\alpha)=M\partial^2_{\beta\beta}\mu \tag{1c}$$

where u_α is the velocity; the index α stands for the Cartesian directions x, y and z; ρ and ν are the density and the kinematic viscosity of the mixture, respectively. Here $P^{th}_{\alpha\beta}$ is the 'thermodynamic' pressure tensor. It contains two parts (Kendon et al., 2001): an isotropic contribution $P\delta_{\alpha\beta}$ that represents the ideal gas pressure and the 'chemical' pressure tensor $P^{chem}_{\alpha\beta}$. The chemical potential in Eq. (1c) is $\mu(\phi)=A\phi-A\phi^3-\kappa\partial^2_{\alpha\alpha}\phi$. Here, $A<0$ and κ are parameters

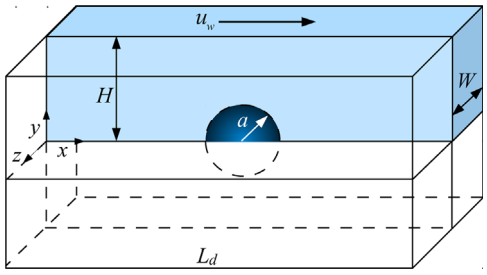

Fig. 1. Simulation domain with the following boundary conditions: $x=0$ and $x=L_d$ are periodic boundaries; $y=0$ has a rotational symmetry boundary condition; $y=H$ is a no-slip wall moving with constant velocity u_w; $z=0$ and $z=-W$ are symmetry planes. At $t=0$ the drop has a spherical shape with initial radius a. Due to the symmetry of the problem only one quarter of the domain needed to be simulated.

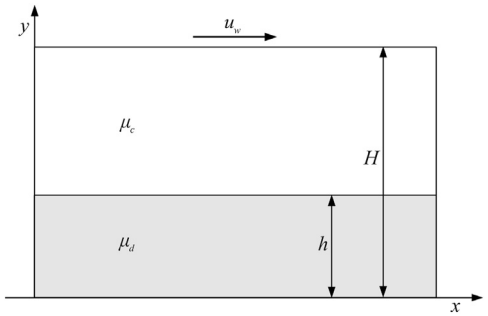

Fig. 2. A slice of the simulation domain at $z=0$ for validation simulations of stratified shear flow; $h=64$ [lu], $H=4\,h$, $\lambda=\mu_d/\mu_c=0.1-2$.

of the free energy model that are related to the surface tension and interface thickness; M is the mobility.

In LBM two particle distribution functions are utilized to solve system (1): one function $f(\boldsymbol{r},t)$ is used to solve the continuity (1a) and Navier–Stokes (1b) equations and the second one $g(\boldsymbol{r},t)$ is used for the convection–diffusion equation (1c). The distribution functions evolve by a time step Δt. All simulations have been performed using a single relaxation time collision operator (Bhatnagar–Gross–Krook (BGK) model Bhatnagar et al., 1954). The discrete lattice Boltzmann equations for the evolution of f and g have the following form:

$$f_q(r_\alpha + c_{\alpha q}\Delta t, t+\Delta t) - f_q(r_\alpha, t) = -\frac{f_q - f_q^{\mathrm{eq}}}{\tau_f},$$
$$g_q(r_\alpha + c_{\alpha q}\Delta t, t+\Delta t) - g_q(r_\alpha, t) = -\frac{g_q - g_q^{\mathrm{eq}}}{\tau_g}, \quad (2)$$

where the index q counts over the number of the discrete velocity directions; f_q^{eq}, g_q^{eq} are the discretized Maxwell–Boltzmann distributions (or equilibrium distributions); $c_{\alpha q}$ denotes the discrete velocity set and τ_f, τ_g are dimensionless relaxation parameters. The equilibrium distributions f_q^{eq}, g_q^{eq} are given in Kusumaatmaja (2008). The D3Q19 lattice is adopted here where $D=3$ denotes three-dimensional flow and $Q=19$ is the number of velocities. In this lattice arrangement, each site communicates with its six nearest and twelve diagonal neighbors. The lattice Boltzmann method operates in dimensionless lattice units (lattice spacing, time step, and lattice density for the length, time and density units, respectively). For the method described here, only uniform cubic lattices can be used; the mesh step Δx is taken as unity, as is the time step Δt.

The distribution functions are defined such that the following summations over all directions q at each lattice point give the local density of the fluid ρ, the local fluid momentum ρu_α and the local order parameter ϕ, respectively:

$$\sum_q f_q = \rho \quad \sum_q c_{\alpha q} f_q = \rho u_\alpha \quad \sum_q g_q = \phi \quad (3)$$

The two liquids have different kinematic viscosities. To implement this, the kinematic viscosity of the mixture ν is set to be a linear function of the order parameter ϕ:

$$\nu(\phi) = \nu_c \frac{\phi_0 - \phi}{2\phi_0} + \nu_d \frac{\phi_0 + \phi}{2\phi_0} \quad (4)$$

where ν_c and ν_d are the kinematic viscosities of continuous and dispersed phases, respectively; and $\phi = \pm\phi_0 = \pm 1$ is the value of the order parameter in the bulk phase on either side of the interface.

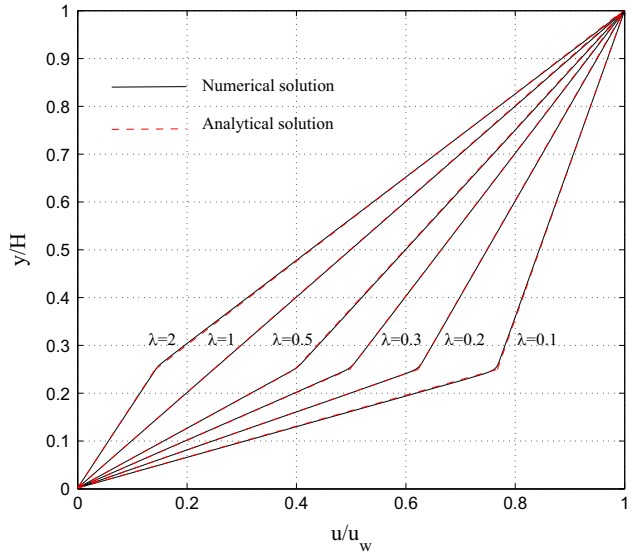

Fig. 3. The x-velocity component as a function of position between the domain center and the sheared plate for different λ in stratified flow; $y/H = 0.25$ is the location of the interface.

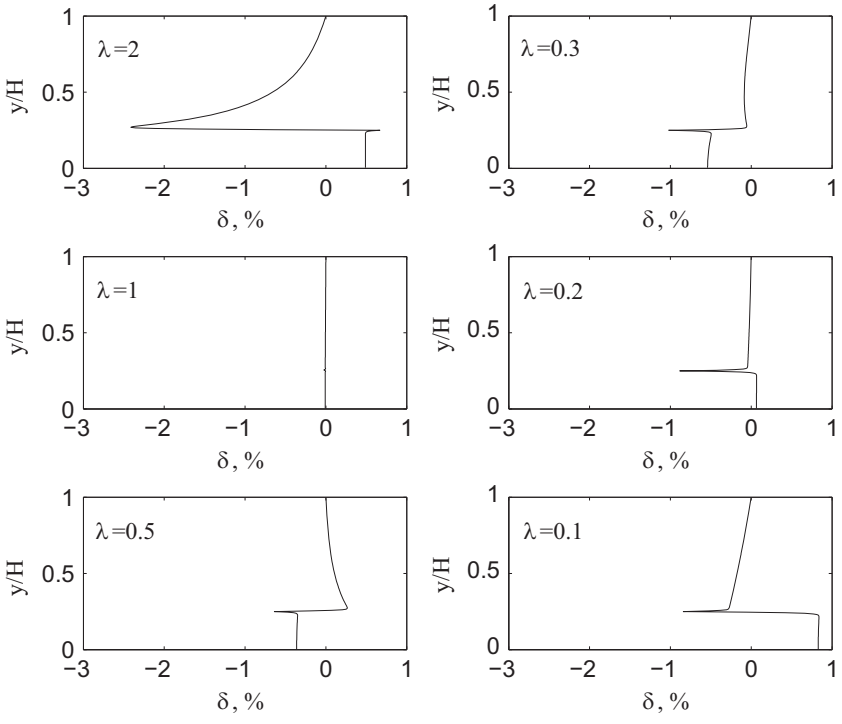

Fig. 4. Relative deviation of x-velocity component in the fluid between numerical and analytical solutions as a function of position between the domain center and the sheared plate for different λ in stratified flow; $y/H = 0.25$ is the location of the interface.

Table 1
Capillary number Ca as a function of viscosity ratio λ at Re = 10.

λ	2.0	1.0	0.5	0.3	0.2	0.15	0.1
Highest subcritical Ca	0.148	0.154	0.163	0.169	0.177	0.183	0.192
Lowest supercritical Ca	0.149	0.155	0.164	0.170	0.178	0.184	0.193
Ca_c (Khismatullin et al., 2003)	0.139	0.147					

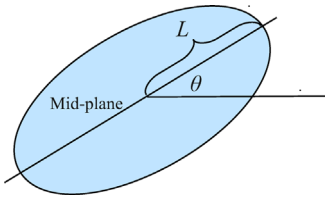

Fig. 5. Definitions of drop elongation L and orientation angle θ.

The relaxation parameter for f_q varies with the composition according to

$$\tau_f(\phi) = \frac{\nu(\phi)}{c_s^2} + \frac{1}{2} \tag{5}$$

Here $c_s^2 = 1/3$ is the speed of sound in lattice units.

The mobility M (see Eq. (1c)) is determined by the coefficient of mobility Γ and the relaxation parameter τ_g according to

$$M = \Gamma\left(\tau_g - \frac{1}{2}\right) \tag{6}$$

For a planar interface, an analytical solution (van der Sman and van der Graaf, 2008) gives the ϕ profile $\phi(x) = \phi_0 \tanh(x/\xi)$ (x is the coordinated normal to the interface). The thickness of the diffuse interface is characterized by a characteristic length ξ:

$$\xi = \left(\frac{2\kappa}{-A}\right)^{1/2}. \tag{7}$$

The interfacial tension σ follows from

$$\sigma = \frac{4}{3}\kappa\frac{\phi_0^2}{\xi}. \tag{8}$$

A simulation code for multiple graphics processing units (GPUs) (Shardt et al., 2013) was used to perform all simulations. The simulation domain is shown in Fig. 1. A symmetry boundary condition through the middle of the domain ($z=0$) and a rotational symmetry boundary condition ($y=0$) were used to avoid unnecessary computations. With these boundary conditions, only a quarter of the full domain was simulated (the highlighted volume in Fig. 1). The shear velocity at $y=H$ was imposed using the method of Ladd (1994). A symmetry condition was used for the phase field ϕ at $y=H$. The boundaries at $z=0$ and $z=-W$ were set as symmetry planes. Periodic boundary conditions were imposed on the $x=0$ and $x=L_d$ planes. Typical processing speeds for the simulations were between 200 and 480 million lattice node updates per second (Mlups) for the smaller and larger domains, respectively.

3. Stratified flow benchmark

Validation simulations were performed to assess the numerical method over the range of viscosity ratios from $\lambda=0.1$ to 2. A stratified sheared flow for which an analytical solution exists was considered. A slice at $z=0$ of a $0.5h \times 4h \times 0.5h$ (x, y, z) simulation domain (where $h=64$ [lu]) is shown in Fig. 2. Only a quarter of the full domain was simulated (rotational symmetry at $y=0$). The full domain therefore represents three sheared liquid layers. The full height of the inner fluid layer is 128 lattice units [lu]. The boundary conditions are the same as described above.

The stratified flow simulations require specification of the following parameters: the interface thickness ξ, the parameters A and κ, the mobility M, and the coefficient of mobility Γ. These parameters were chosen to be the same as for a sheared drop (that will be considered later) and then used in the benchmark simulations to assess the accuracy of simulations with these parameters.

The procedure for selecting the numerical parameters according to the guidelines of Komrakova et al. (2014) is as follows. First, the drop resolution is specified: the drop radius is chosen to be 64 lattice units to perform high-resolution simulations that can resolve the satellite and sub-satellite drops formed after breakup. This drop size requires an interface thickness of at least two lattice units (Komrakova et al., 2014), and therefore $\xi=2$ [lu] is chosen. Consequently, the Cahn number is $Ch=0.03$. The second step is to determine the Peclet number, which requires specifying several parameters. The relaxation time of the continuous fluid phase is kept constant at $\tau_f=0.7$ which specifies a continuous phase viscosity of $\nu_c=1/15$ [lu]. The shear rate $\dot{\gamma}$ follows from the Reynolds number, which is 10 in the present study: $\dot{\gamma} = \mathrm{Re}\,\nu_c/a^2$. The interfacial tension σ is determined by the capillary number: $\sigma = a\dot{\gamma}\mu_c/\mathrm{Ca}$ (where $\mu_c = \rho\nu_c$ and the uniform density $\rho=1$ in lattice units). To determine Pe, an estimate of the typical Ca is needed, which is not known yet, as the critical capillary number is an output of the simulation. For an initial estimate, $\mathrm{Ca}=0.15$ is used, which is the near-critical value for $\lambda=1$ reported by Khismatullin et al. (2003). The interfacial tension σ and interface thickness ξ give the value of κ (see (8)): $\kappa = 3\sigma\xi/(4\phi_0^2)$. Finally, with κ and ξ specified, the value of the parameter A is (see Eq. (7)): $A = 2\kappa/\xi^2$. Thus only one parameter remains to be specified in the Peclet number – the mobility M which is determined by the mobility coefficient Γ. Every simulation in the present study was performed with the relaxation time for the phase field $\tau_g=1$ which implies that $M=\Gamma/2$ (see Eq. (6)). Consequently, $Pe = 12.0/\Gamma$. As shown in Komrakova et al. (2014), to perform stable simulations the mobility coefficient should be chosen in the range 1–15. Furthermore, it was outlined that for the case at $\mathrm{Re}=10$, $\mathrm{Ca}=0.15$ and $\lambda=1$, $Pe>4$ yields results that agree well with reference data. For that reason it was decided to set the Peclet number to $Pe=6$. Therefore, $\Gamma=2$ was used in the benchmark simulations.

The x-velocity component in the fluid as a function of y (see Fig. 2) for different viscosity ratios λ is presented in Fig. 3. The relative deviation of velocity values from the analytical solution ($\delta = |u_{\mathrm{analytical}} - u_{\mathrm{numerical}}|/u_{\mathrm{analytical}} \times 100\%$) is shown in Fig. 4. Calculation of δ with $u_{\mathrm{analytical}}=0$ was not performed because the first node in the y-direction is located half a lattice spacing from the boundary. As one can see, the overall largest deviation occurs with $\lambda=2$ which is 2.5% and happens on the interface. For the rest of the λ values, the relative deviation from the analytical solution is within $\pm 1\%$. It is concluded that the method can deal with viscosity ratios $0.1 \le \lambda \le 2$ in a consistent manner.

4. Results

The simulations to determine critical capillary numbers were performed with an initial drop radius $a=64$ lattice units in a $16a \times 4a \times 2a$ (x, y, z) domain (a quarter of the full domain). The height $2H = 8a$ of the domain is the same as used in the reference

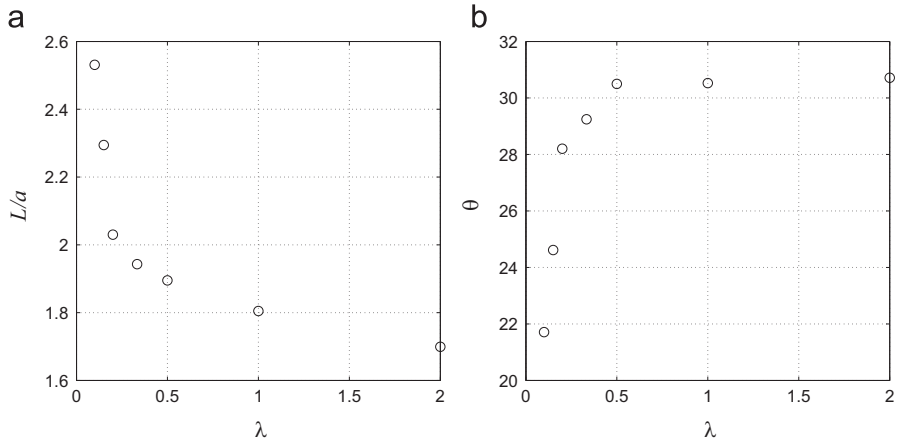

Fig. 6. Drop deformation results at Re=10. The L/a ratio (a) and the orientation angle θ, (deg) (b) as a function of viscosity ratio λ at the highest subcritical Ca.

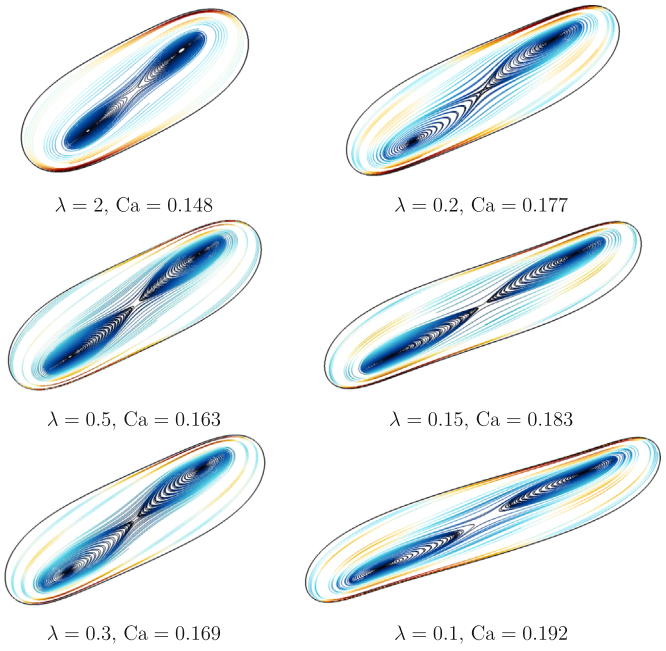

Fig. 7. Drop shape and internal circulations at Re=10 and the highest subcritical capillary number for each viscosity ratio λ. The color of the streamlines shows the speed based on $x-$ and $y-$ velocity components in the $(x-y)$ section (see Fig. 1) and varies from minimum (dark blue) to maximum (dark red) values. (For interpretation of the references to color in this figure caption, the reader is referred to the web version of this article.)

simulations of Khismatullin et al. (2003). Additionally, the influence of the proximity of walls was considered in Komrakova et al. (2014) and it was shown that $H=4a$ is sufficient to avoid confinement effects. The thickness of the interface was two lattice units so that $Ch=0.03$. The diffusion coefficient Γ was set to 2 (as in the benchmark). This gives Peclet numbers in the range 5–8 depending on the capillary number specified for each simulation. The reference data presented by Khismatullin et al. (2003) for $\lambda=1$ and 2 were used for validation.

Two capillary numbers were searched for every λ: one for which the droplet does not break and attains a steady state (highest subcritical Ca) and the second one for which the drop breaks into fragments (lowest supercritical). The critical capillary number is determined as the arithmetic average of these two values. The results are presented in Table 1. The relative deviation of Ca_c from the reference data is 5 and 7% for $\lambda=1$ and 2, respectively. For λ in the range 0.1–2, the critical capillary number increases as the viscosity ratio decreases. This observation is in line with reference data. For instance, Khismatullin et al. (2003) reported that at Re=10 the critical capillary number has a minimum close to $\lambda=3$. Thus Ca_c increases as λ decreases starting from a value of 3.

In the literature, two parameters are used to measure the deformation of the drop when a steady shape exists: the Taylor deformation parameter and the orientation angle (Taylor, 1932, 1934). Inertia (which is relevant for shear with Re=10) changes the steady shape of drops from ellipsoidal (in creeping flow) to elongated. Moreover, the symmetry over the mid-plane of the drop (see Fig. 5) might be lost. For that reason in this work the ratio of maximum elongation to initial undeformed drop radius L/a is used to characterize the deformation instead of the Taylor deformation parameter. The second parameter is the orientation angle θ of the drop. The maximum elongation of the drop is the length of the line that connects two points at the tips of the drop located at the maximum distance apart. The angle of inclination (or orientation angle) is accordingly measured between this line and the horizontal axis.

The drop deformation at the highest subcritical capillary numbers for different viscosity ratios is presented in Fig. 6. As the viscosity ratio decreases the drop becomes more elongated (Fig. 6(a)). The inclination angle decreases as λ decreases (Fig. 6(b)).

The steady shape of the drop and internal circulations at the highest subcritical capillary numbers for each viscosity ratio are depicted in Fig. 7. At $\lambda=2$ the shape of the drop is almost symmetrical over the mid-plane; but the tips of the drop are slightly tilted away from the mid-plane. The drop has a 'capsule' shape. At Re=10 (unlike creeping flow) two vortices develop inside the drop over the entire range of λ. As λ decreases, the drop becomes more elongated and less symmetrical over the mid-plane. In addition, the drop becomes more deformable, and the internal circulations follow the pattern of the drop shape. At a viscosity ratio of 0.1, the tips of the drop are clearly tilted away from the mid-plane. The symmetry across the mid-plane is lost. It should be noted that the deformation parameters (Fig. 6) and the shape of the drop (Fig. 7) depend on how close the specified capillary number is to the critical value. However the trends of L/a and θ as functions of λ remain the same.

The viscosity ratio λ also significantly affects the breakup process. Consider the differences in the breakup process between $\lambda=2$ (Fig. 8) and 0.1 (Fig. 10) at the lowest supercritical capillary numbers. The evolution of drop shape and velocity field for $\lambda=2$ at Ca=0.149 is depicted in Fig. 8. By the time instant $\bar{t}=19.9$, the shape of the drop is almost ellipsoidal, and only one vortex has formed inside the drop. By $\bar{t}=39.4$, the drop becomes elongated. Starting from this time, two

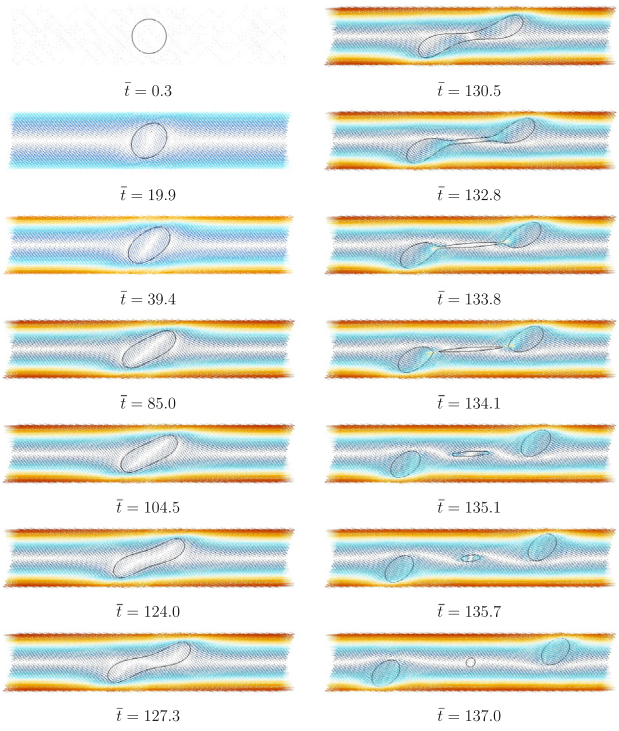

Fig. 8. Drop shape and velocity field over time at the lowest supercritical capillary number Ca = 0.149, Re = 10, λ=2 ($\bar{t} = t\dot{\gamma}$). The images show ~40% of the full domain height. Color indicates velocity magnitude from lowest (dark blue) to highest (dark red). (For interpretation of the references to color in this figure caption, the reader is referred to the web version of this article.)

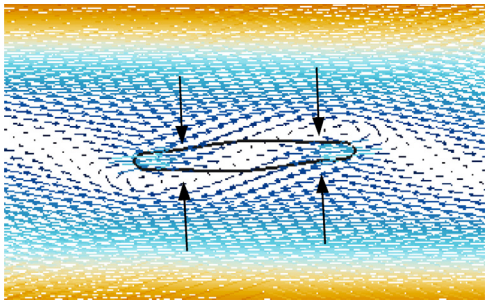

Fig. 9. Enlarged image of satellite drop shape and velocity field at Ca = 0.149, Re = 10, λ=2 and $\bar{t} = 135.1$ showing a tendency to form two sub-satellite drops due to formation of bridges at the locations indicated by the arrows.

vortices form and they become fully-developed by $\bar{t} = 85.0$. The drop starts necking in the middle at about $\bar{t} = 104.5$. The shape of the drop changes from elongated to dumbbell. The drop continues to stretch while thinning its center portion. Eventually a thin bridge develops that connects two 'bulbs' formed at the ends of the drop (see time instant $\bar{t} = 132.8$). Further shearing of the drop leads to the 'bulbs' pinching off, forming two daughter droplets and one satellite between them ($\bar{t} = 134.1$). When the satellite drop retracts at $\bar{t} = 135.1$ a tendency to form two sub-satellite droplets can be seen (see the enlarged image in Fig. 9). However, the satellite drop retracts faster than the two bridges thin. Finally only one satellite drop appears ($\bar{t} = 135.7$). After breakage, the satellite drop stays stationary, while the daughter droplets move away ($\bar{t} = 137.0$). This drop breakup mechanism has been called end-pinching (Marks, 1998; Stone et al., 1986; Zhao, 2007).

The evolution of drop shape and velocity field when the viscosity ratio is λ=0.1 at Ca=0.193 is shown in Fig. 10. Two vortices form inside the drop right from the beginning ($\bar{t} = 18.2$). By the time instant $\bar{t} = 65.4$, the drop elongates and loses symmetry over the

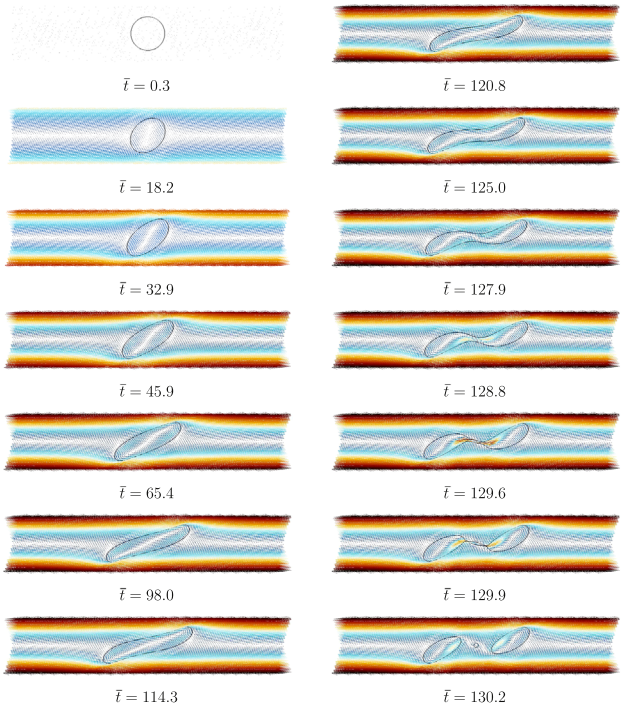

Fig. 10. Drop shape and velocity field over time at the lowest supercritical capillary number Ca = 0.193, Re = 10, λ=0.1. The images show ~40% of the full domain height. Color indicates velocity magnitude from lowest (dark blue) to highest (dark red) values. (For interpretation of the references to color in this figure caption, the reader is referred to the web version of this article.)

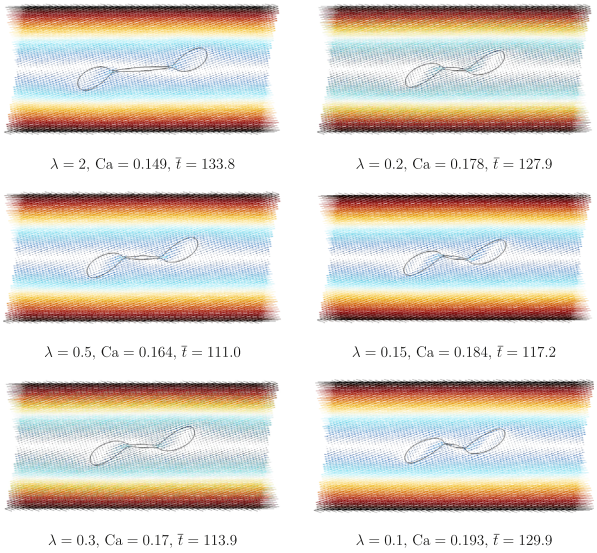

Fig. 11. Drop shape and velocity field for different viscosity ratios at Ca ~ Ca_c (the lowest supercritical value) just before breakup. Color indicates velocity magnitude from lowest (dark blue) to highest (dark red) values. (For interpretation of the references to color in this figure caption, the reader is referred to the web version of this article.)

mid-plane. The drop elongation slows down starting at $\bar{t} = 98.0$. At $\bar{t} = 114.3$ the drop starts rotating clockwise away from the axis of elongation. The central part of the drop is completely aligned with the flow at $\bar{t} = 125.0$. After that it continues to rotate and thins. By the time instant $\bar{t} = 128.8$ a bridge that connects the 'bulbs' of the drop is formed. During the thinning of the bridge, the 'bulbs' of the drop move slowly away from each other. Finally, the bridge breaks. Three fragments are formed: two daughter droplets and one satellite drop between them ($\bar{t} = 130.2$).

Table 2
Ratio of daughter drop volume V_d to the critical drop volume V_c as a function of mother drop radius a relative to the critical drop radius a_c.

a/a_c	1.01	1.1	1.2	1.3
V_d/V_c	0.43	0.55	0.67	0.76

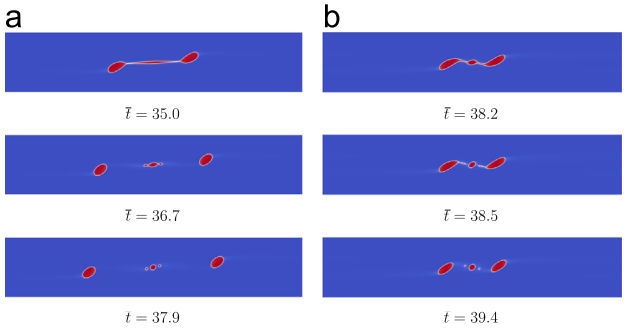

Fig. 12. Drop breakup process at $Ca = 1.2Ca_c$: (a) $\lambda=2$; $Ca = 0.178$, (b) $\lambda=0.1$; $Ca = 0.231$.

Table 3
Effect of mesh resolution.

Drop radius a, (lu)	$\lambda=0.1$		$\lambda=2$	
	48	64	48	64
Highest subcritical Ca	0.191	0.192	0.151	0.148
Lowest supercritical Ca	0.192	0.193	0.152	0.149

For every viscosity ratio $\lambda=2$, 1, 0.5, 0.3, 0.2, 0.15, and 0.1 only three fragments form after breakup at $Ca \sim Ca_c$ by the end-pinching mechanism: two daughter droplets and one satellite between them. In general, at higher λ the drop is more elongated before breakup. However, drop elongation before breakup strongly depends on how close the specified capillary number is to the critical value which is discussed, for instance, in Bławzdziewicz et al. (2002), Cristini et al. (2003) and Cristini and Renardy (2006). Fig. 11 shows the drop shape and velocity field for different λ at the time just before breakup. When $\lambda=2$ the angle between the bridge and x-direction is sharp. When $\lambda=0.5$ the bridge is horizontal. For smaller viscosity ratios the bridge forms an obtuse angle with the x-direction. The volume of the bridge decreases as the viscosity ratio decreases, making smaller satellite drops after breakup.

For every viscosity ratio the initial elongation process (from the beginning of deformation up to the moment of neck formation) is slow. Once the neck in the middle of the drop starts to form, the elongation rate increases. The same observations were reported by Stone et al. (1986) who investigated drop behavior in a linear two-dimensional flow under creeping flow conditions.

To further test the capabilities of the numerical technique, one can consider the breakup of initial (mother) drops of varying volumes under constant shearing conditions, i.e. $\dot{\gamma} = \text{const}$ which requires $\text{Re} = K\text{Ca}^2$ where K is a constant. This problem has been numerically simulated by Renardy and Cristini (2001a, 2001b), Renardy et al. (2002) and Khismatullin et al. (2003) who showed that for the viscosity ratio $\lambda=1$ the daughter drop volume saturates to a fraction of the critical volume as the mother drop size increases. To avoid the computational expense of simulating domains of increasing size, which scale as a^3 with the mother drop radius, one can keep the size of the mother drop constant while changing the dimensionless parameters (Re, Ca, *Pe*, *Ch*) appropriately. With this approach the resolution of the drops remains constant as a/a_c increases. The results of the simulations of the case with $\lambda=1$ and an undeformed mother drop size $a=64$ [lu] are listed in Table 2. As one can see, V_d/V_c increases with a/a_c just as it does in Khismatullin et al. (2003) at $\text{Re}=1$ and $\text{Re}=50$. The saturation is not as clear as in Khismatullin et al. (2003) which could be due to inadequate resolution in the neck region and of the daughter drops as a/a_c increases. With increasing a/a_c (i.e. the capillary number Ca) the fraction of the mother drop volume in the neck region increases making the resolution of this slender region more important (see the difference between the neck regions in Figs. 11 and 12).

As demonstrated, for instance, by Zhao (2007) for creeping flow, the breakup process depends on the viscosity ratio and capillary number. Thus it is of interest to see these dependencies for $\text{Re}=10$. Therefore the cases with $\lambda=2$ and 0.1 have been studied at $\text{Ca} = 1.2\text{Ca}_c$, $\text{Ca} = 1.5\text{Ca}_c$, and $\text{Ca} = 2\text{Ca}_c$ (and as before $\text{Re}=10$). Based on the experimental observations of Zhao (2007) and our results with $\text{Ca} \sim \text{Ca}_c$ at $\lambda=2$, at higher supercritical capillary numbers the drop will elongate more before breakup. Due to the larger elongation, longer simulation domains are required. Unless otherwise stated, the simulations were performed in $40a \times 4a \times 2a$ domains (a quarter of the full domain) with an initial undeformed drop radius $a=48$ [lu] and interface thickness $\xi=2$ [lu] (the Cahn number $Ch=0.04$). The mobility coefficient Γ varied from 2 to 6 to keep the Peclet number in the range 5–7.

To assess the accuracy of the method at the lower mesh resolution (drop radius $a=48$ [lu]; previously it was 64) the critical Ca for $\lambda=0.1$ and 2 were determined and compared to the higher resolution results. The comparison is presented in Table 3. The deviation of Ca_c obtained at $a=48$ and 64 is 0.5% and 2% for $\lambda=0.1$ and 2, respectively. Good agreement is therefore demonstrated, and the lower resolution was used for further studies. Since the critical capillary numbers determined at higher mesh resolution are more accurate, their values were used in setting Ca in the simulations at the higher supercritical capillary numbers.

Drop breakup at $\text{Ca} = 1.2\text{Ca}_c$ for $\lambda=2$ and 0.1 is shown in Fig. 12(a) and (b), respectively. The deformation happens in the same manner as it does at the lowest supercritical capillary number. The drop breaks by the end-pinching mechanism. In both cases five fragments are formed after breakup. Two sub-satellites appear upon retraction of the satellite drop after the bridge breaks. Additionally, the drops are broken at different angles: compare the location of the daughter drops and sub-satellites for $\lambda=2$ and 0.1 at the last frames in Fig. 12.

Zhao (2007) experimentally investigated drop breakup in dilute Newtonian emulsions in simple shear creeping flow over a wide range of viscosity ratios ($0.0017 < \lambda < 3.5$). It was demonstrated that a drop at $\text{Ca} \gtrsim \text{Ca}_c$ is broken under steady shear by the end-pinching mechanism into two equal sized daughter drops (and possible satellite and sub-satellites) for the entire range of viscosity ratio studied. Our results of drop deformation and breakup at the higher Reynolds number of $\text{Re}=10$ at $\text{Ca} \sim \text{Ca}_c$ and $\text{Ca} = 1.2\text{Ca}_c$ are in line with these observations at lower Re. However, inertia changes the initial stages of drop deformation: it induces two vortices inside the drop and the drop loses its symmetry across the mid-plane. In contrast to this, under creeping flow conditions the initially spherical drop is deformed into an ellipsoid. The rest of the breakup process occurs in the same manner in both cases: the drop stretches forming a neck in the middle. Eventually the neck breaks after thinning and the drop disintegrates into two daughter drops separated by smaller satellite and sub-satellite drops. In addition it was outlined by Zhao (2007) that as λ decreases, the ends of the deformed drop become more slender and increasingly pointed. Similar behavior is seen at our higher Reynolds number (compare the drop ends in Fig. 11 for $\lambda=2$ and $\lambda=0.1$).

The drop breakup processes at $\text{Ca} = 1.5\text{Ca}_c$ when $\lambda=2$ and 0.1 are presented in Fig. 13(a) and (b), respectively. The initial drop

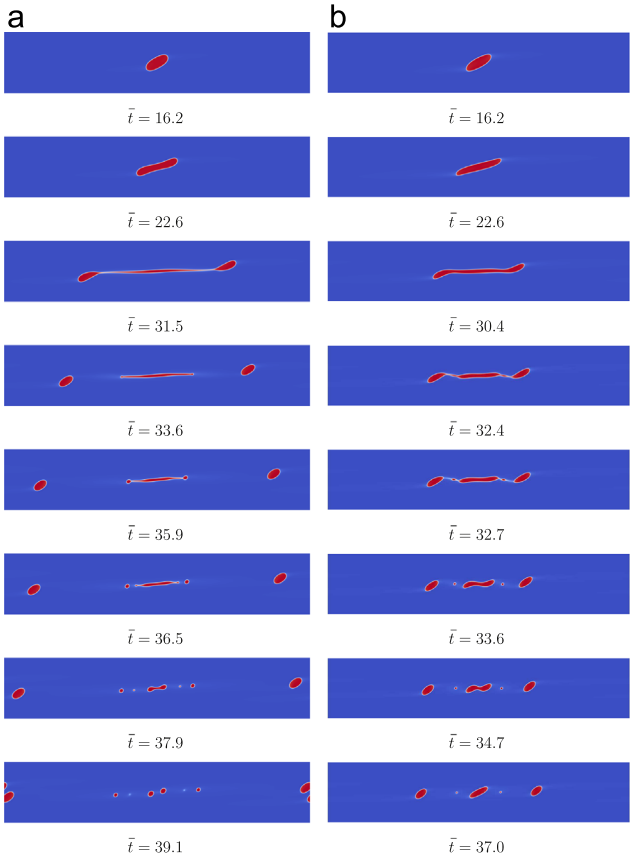

Fig. 13. Drop breakup process at $Ca = 1.5Ca_c$: (a) $\lambda=2$; $Ca = 0.223$, (b) $\lambda=0.1$; $Ca = 0.289$.

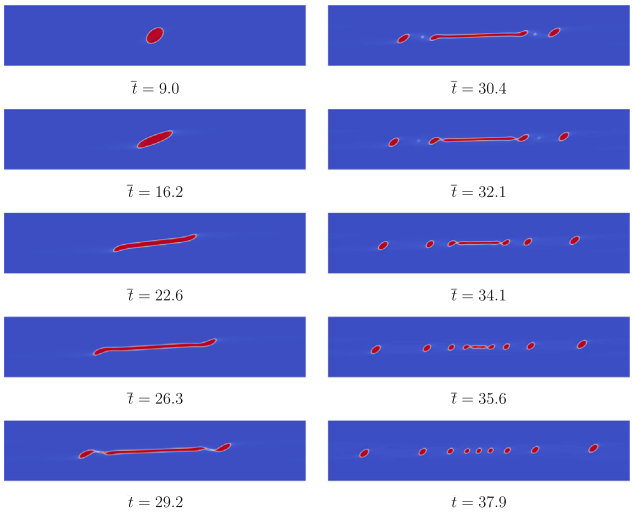

Fig. 14. Drop breakup process at $Ca = 2Ca_c = 0.385$ and $\lambda=0.1$.

deformation happens in the same manner as it does for lower capillary numbers for each viscosity ratio. At $\bar{t} = 22.6$ the drop with $\lambda=2$ starts necking while the drop when $\lambda=0.1$ is still elongating. Because of the high viscosity of the dispersed phase ($\lambda=2$), the drop is significantly stretched. As a result the bridge thins forming two necks ($\bar{t} = 31.5$), and then the drop ends pinch off ($\bar{t} = 33.6$). The daughter droplets move away from each other. The central thread retracts after breakup, forming satellite drops at both ends ($\bar{t} = 35.9$). At later time, the thread is broken by the end-pinching mechanism. In the end, eight fragments are produced after breakup ($\bar{t} = 39.1$). When $\lambda=0.1$, the drop is less elongated

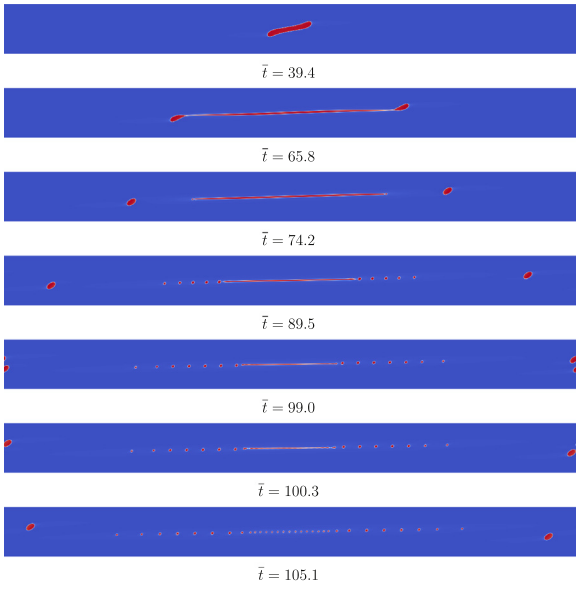

Fig. 15. Drop breakup process at $Ca = 2Ca_c = 0.297$ and $\lambda=2$.

compared to the case with $\lambda=2$. After the first breakup event ($\bar{t} = 32.7$) the fragments move slowly away from each other while the central portion of the drop retracts. The neck formed in the middle ($\bar{t} = 34.7$) is not thin enough to break. Eventually only five fragments are formed. Thus shear of a more viscous drop at $Ca = 1.5Ca_c$ produces more drops than shear of a less viscous drop. In addition, daughter droplets move away faster from each other when $\lambda=2$ compared to $\lambda=0.1$.

It is necessary to note that small satellite and especially sub-satellite drops disappear quickly after formation (e.g. see Fig. 13(a) frames at $\bar{t} = 37.9$ and $\bar{t} = 39.1$). That means higher mesh resolution, i.e. larger initial drop radius in lattice units, is required to resolve drops of this size (see Komrakova et al., 2014 for details, where it was shown that increasing resolution allows smaller drops relative to the initial drop size to remain). Additionally, the domain length for the case with $\lambda=2$ is not enough (the drop wraps around the ends of the periodic domain, see last frame in Fig. 13(a)). Nevertheless, the drop breakup in the domain center is not affected by this event.

The drop breakup process at $Ca = 2Ca_c$ and $\lambda=0.1$ is shown in Fig. 14. The drop is broken into nine fragments by repetition of the end-pinching mechanism. As noted by Zhao (2007) in Stokes flow, the drops deform into longer threads with increasing capillary number. The same conclusion holds at $Re = 10$ for viscosity ratios of 0.1 and 2.

If a drop with $\lambda=2$ is sheared at $Ca = 2Ca_c$, significant elongation is expected before breakup. Moreover, a thin cylindrical thread is expected to appear. In order to resolve small fragments and avoid influence of horizontal periodicity, it is necessary to run this simulation in a longer domain and with a higher mesh resolution. Therefore an undeformed drop radius of $a=64$ [lu] and a $91.5a \times 4a \times 2a$ simulation domain were chosen. The results are presented in Fig. 15. As expected, the high λ and Ca values cause the formation of a long thin thread that connects the drop ends ($\bar{t} = 65.8$). After the first breakup by end-pinching, two daughter droplets appear. Next, the thread breaks by the end-pinching mechanism again, producing drops of almost equal size but slightly smaller compared to the first drops. Eventually, the cylindrical thread stretches sufficiently that capillary wave breakup occurs ($\bar{t} = 100.3$) due to the growth of axial fluctuations in the thread diameter (Marks, 1998). Moreover, this event produces drops of equal size ($\bar{t} = 105.1$). Enlarged images of the capillary wave breakup event are presented in Fig. 16.

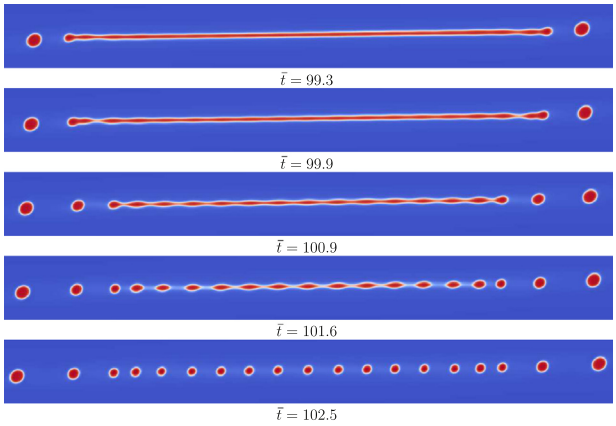

Fig. 16. Capillary wave breakup at $Ca = 2Ca_c$ and $\lambda = 2$ (the images show a portion of the full domain).

5. Conclusions

A free energy lattice Boltzmann method was used to perform three-dimensional simulations of single liquid drops suspended in another liquid and subjected to simple shear flow. The guidelines presented by Komrakova et al. (2014) were used to choose the parameters of the numerical method. In this paper, the influence of dispersed phase viscosity on the behavior of sheared drops with inertia ($Re = 10$) was investigated.

A validation simulation of stratified shear flow was conducted to show that the numerical method can handle viscosity ratios (dispersed phase viscosity over continuous phase viscosity) in the range $\lambda = 0.1 - 2$. The results at worst deviated 2.5% from the analytical solution at $\lambda = 2$ and were within 1% for the rest of the λ values.

High resolution simulations were performed over the range of viscosity ratios $\lambda = 0.1$–2 at different capillary numbers. The critical capillary number Ca_c for every λ was determined. The Ca_c value decreases as λ increases. At the highest subcritical capillary number, the drop becomes less elongated and more oriented towards the vertical axis with increasing viscosity ratio. Unlike creeping flow, at $Re = 10$ two vortices form inside the drop and loss of symmetry across the mid-plane of the drop is observed.

The results show how the breakup process depends on the viscosity ratio and the capillary number. High λ values result in significant drop elongation before breakup. However, the elongation depends on the specified capillary number. Drop breakup due to end-pinching was observed in every simulation performed: 'bulbs' form at the ends of the stretched drop and eventually pinch off. The first breakup event produces the largest daughter droplets for every viscosity ratio considered. Depending on the volume of the center portion of the drop, further breakups might occur. The number of fragments is a function of the viscosity ratio and capillary number. As Ca increases the number of produced fragments increases. More fragments are formed for higher λ at a given ratio between specified capillary number and the critical capillary number corresponding to each λ. For $\lambda = 0.1$ drops only break by the end-pinching mechanism at $Ca_c \le Ca \le 2Ca_c$. When $\lambda = 2$ at $Ca = 2Ca_c$ the thread becomes sufficiently elongated that capillary wave breakup occurs. Thus the necessary condition for the capillary wave breakup is a sufficiently high capillary number (for given λ) to stretch the drop to a sufficient thinness. For the low viscosity ratio $\lambda = 0.1$, $Ca = 2Ca_c$ is insufficient to break the drop by the capillary wave breakup mechanism.

At the lowest supercritical capillary number, the rate of drop elongation during the initial stage of deformation increases as λ decreases. The time needed to break the drop is related to the orientation of the bridge that connects the ends of the drop. The bridge volume decreases as λ decreases.

The results of the present study can find industrial applications, such as in the production and processing of emulsions and liquid–liquid dispersions. In these processes, the drop size distribution of the final product is of great importance. The proposed numerical method could be used to determine the drop size distribution (DSD) of given liquids and shearing conditions. Alternatively, the shearing conditions required for a desired DSD can be estimated. For instance, capillary wave breakup produces drops of equal size. Knowledge of the conditions when this breakup mechanism occurs may improve the efficiency of monodisperse emulsion production. Moreover, the sizes of the daughter droplets formed as a result of the breakage event for $\lambda = 0.1$ at $Ca = 2Ca_c$ are also nearly monodisperse. This phenomenon can be used for production of monodisperse emulsions in a device as simple as a colloid mill, representing a narrow gap Taylor–Couette device.

References

Badalassi, V.E., Ceniceros, H.D., Banerjee, S., 2003. Computation of multiphase systems with phase field models. J. Comput. Phys. 190, 371–397.
Bhatnagar, P.L., Gross, E.P., Krook, M., 1954. A model for collision processes in gases. I. Small amplitude processes in charged and neutral one-component systems. Phys. Rev. 94, 511–525.
Bławzdziewicz, J., Cristini, V., Loewenberg, M., 2002. Critical behavior of drops in linear flows: I. Phenomenological theory for drop dynamics near critical stationary states. Phys. Fluids 14, 2709–2718.
Boxall, J., Koh, C., Sloan, E., Sum, A., Wu, D., 2011. Droplet size scaling of water-in-oil emulsions under turbulent flow. Langmuir 28, 104–110.
Cahn, J.W., Hilliard, J.E., 1958. Free energy of a nonuniform system. I. Interfacial free energy. J. Chem. Phys. 28, 258–267.
Cahn, J.W., Hilliard, J.E., 1959. Free energy of a nonuniform system. III. Nucleation in a two–component incompressible fluid. J. Chem. Phys. 31, 688–699.
Cristini, V., Renardy, Y., 2006. Scalings for droplet sizes in shear-driven breakup: non-microfluidic ways to monodisperse emulsions. FDMP: Fluid Dyn. Mater. Process. 2, 77–93.
Cristini, V., Guido, S., Alfani, A., Bławzdziewicz, J., Loewenberg, M., 2003. Drop breakup and fragment size distribution in shear flow. J. Rheol. 45, 1283–1298.
Ding, H., Spelt, P.D.M., Shu, C., 2007. Diffuse interface model for incompressible two-phase flows with large density ratios. J. Comput. Phys. 226, 2078–2095.
Fjelde, I., 2007. Formation damages caused by emulsions during drilling with emulsified drilling fluids. Soc. Pet. Eng. 105858, 1–8.
Grace, H., 1982. Dispersion phenomena in high viscosity immiscible fluid systems and application of static mixers as dispersion devices in such systems. Chem. Eng. Commun. 14, 225–277.
Jacqmin, D., 1999. Calculation of two–phase Navier–Stokes flows using phase–field modeling. J. Comput. Phys. 155, 96–127.
Kendon, V.M., Cates, M.E., Pagonabarraga, I., Desplat, J.-C., Bladon, P., 2001. Inertial effects in three-dimensional spinodal decomposition of a symmetric binary fluid mixture: a lattice Boltzmann study. J. Fluid Mech. 440, 147–203.
Khismatullin, D.B., Renardy, Y., Cristini, V., 2003. Inertia-induced breakup of highly viscous drops subjected to simple shear. Phys. Fluids 15, 1351–1354.
Komrakova, A., Shardt, O., Eskin, D., Derksen, J., 2014. Lattice Boltzmann simulations of drop deformation and breakup in shear flow. Int. J. Multiph. Flow 59, 24–43.
Kusumaatmaja, H., 2008. Lattice Boltzmann Studies of Wetting and Spreading on Patterned Surfaces (Ph.D. thesis), University of Oxford.
Ladd, A.J.C., 1994. Numerical simulations of particulate suspensions via a discretized Boltzmann equation—Part I. Theoretical foundation. J. Fluid Mech. 271, 285–309.
Marks, C.R., 1998. Drop Breakup and Deformation in Sudden Onset Strong Flows (Ph.D. thesis), University of Maryland.
Penrose, O., Fife, P.C., 1990. Thermodynamically consistent models of phase-field type for the kinetics of phase transitions. Physica D 43, 44–62.
Rallison, J., 1984. The deformation of small viscous drops and bubbles in shear flow. Ann. Rev. Fluid Mech. 16, 45–66.
Renardy, Y.Y., Cristini, V., 2001a. Effect of inertia on drop breakup under shear. Phys. Fluids 13, 7–13.
Renardy, Y.Y., Cristini, V., 2001b. Scalings for fragments produced from drop breakup in shear flow with inertia. Phys. Fluids 13, 2161–2164.
Renardy, Y., Cristini, V., Li, J., 2002. Drop fragment distributions under shear with inertia. Int. J. Multiphase Flow 28, 1125–1147.
Rueger, P., Calabrese, R., 2013. Dispersion of water into oil in a rotor-stator mixer. Part 1: Drop breakup in dilute systems. Chem. Eng. Res. Des. 91, 2122–2133.
Rumscheidt, F., Mason, S.G., 1961. Particle motions in sheared suspensions. XII. Deformation and burst of fluid drops in shear and hyperbolic flow. J. Colloid Sci. 16, 238–261.
Shardt, O., Derksen, J., Mitra, S., 2013. Simulations of droplet coalescence in simple shear flow. Langmuir 29, 6201–6212.

Stone, H.A., 1994. Dynamics of drop deformation and breakup in viscous fluids. Annu. Rev. Fluid Mech. 26, 65–102.
Stone, H., Bentley, B., Leal, G., 1986. An experimental study of transient effects in the breakup of viscous drops. J. Fluid Mech. 173, 131–158.
Swift, M.R., Orlandini, E., Osborn, W.R., Yeomans, J.M., 1996. Lattice Boltzmann simulations of liquid–gas and binary fluid systems. Phys. Rev. E 54, 5041–5052.
Taylor, G.I., 1932. The viscosity of a fluid containing small drops of another fluid. Proc. R. Soc. Lond. A 138, 41–48.
Taylor, G.I., 1934. The formation of emulsions in definable fields of flow. Proc. R. Soc. Lond. A 146, 501–523.
van der Sman, R.G.M., van der Graaf, S., 2008. Emulsion droplet deformation and breakup with Lattice Boltzmann model. Comput. Phys. Commun. 178, 492–504.
Yue, P., Feng, J.J., Liu, C., Shen, J., 2004. A diffuse-interface method for simulating two-phase flows of complex fluids. J. Fluid Mech. 515, 293–317.
Zhao, X., 2007. Drop breakup in dilute Newtonian emulsions in simple shear flow: new drop breakup mechanisms. J. Rheol. 51, 367–392.